MAGNETIC AND MICROSTRUCTURE PROPERTIES OF RAPIDLY QUENCHED TRANSITION-METAL-RARE-EARTH-INTERMETALLICS WITH $ThMn_{12}$ STRUCTURE

by

ERIC WALTER SINGLETON

B.A., Hastings College, 1986

A THESIS

submitted in partial fulfillment of the

requirements for the degree

MASTER OF SCIENCE

Department of Physics

KANSAS STATE UNIVERSITY

Manhattan, Kansas

1988

Approved by:

George Hadjipanayis

Major Professor

ACKNOWLEDGEMENTS

I am thankful for all of the instructors over the years who have shared with me their knowledge which has enabled me to do this research. I am especially indebted to Dr. G.C. Hadjipanayis who supervised this research project. His insight and encouragement were invaluable and is greatly appreciated.

Thanks also to Dr. Jan Strzeszewski and Larry Seib for their assistance in obtaining results using the electron microcsope. I also wish to thank the students in our research group for their assistance in the lab. The techniques which they helped me learn were quite valuable.

Special thanks are due to Mary C. Kinsey for her assistance in typing the manuscript, and for her constant love and support over the period of this research.

List of Figures

Figure

List of Tables

Table

Chapter 1

THEORETICAL CONCEPTS

1.1. Introduction

The search for permanent magnets has had a very long history, beginning with the first magnetic material known to man, magnetite (Fe_3O_4) which was used by the Greeks. It has also been found that the Chinese used a compass as early as 2500 B.C. The compass was also very important to early European navigators as is reflected in the old English word lodestone for magnetite; it means *waystone*, because it points the way[1].

Since this early time, the uses for permanent magnetic materials has grown at a rate equal to or exceeding our ability to provide new materials for use. Thus, the search for new permanent magnet materials continues. The most widely used permanent magnet materials prior to the early 1980's were the cobalt containing $SmCo_5$ and Alnico magnets. These magnets were costly due to the strategic importance of cobalt and the low supply of samarium. Then, in 1983 a breakthrough in the development of new permanent magnet materials took place when Hadjipanayis *etal*[3] reported the first noncobalt containing magnet, FePrBSi with a coercive field of 15kOe and an energy product of 13MGOe. Croat[4] and Koon[5] soon reported similar results, and Masato Sagawa[6] of the Sumitomo Special Metals Company of Japan revealed the making of an anisotropic magnet of Fe-Nd-B with an energy product of 36MGOe by conventional powder metallurgical techniques.

The discovery of the $Nd_2Fe_{14}B$ permanent magnets has led to the realization that novel materials may be found from the large group of ternary phases that may form when iron and rare earths are combined with some third component. In the following research a newly found ternary Fe-rich system of compounds is characterized which is formed when iron and rare earth elements are combined with small amounts of several intermetallics.

1.2. Distinct Properties of Ferromagnets

Ferromagnetic materials consist of a large number of materials all having certain similar yet distinct properties. The first of these is that below a certain critical temperature, the Curie temperature, a ferromagnet becomes spontaneously magnetized. The magnetization increases with decreasing temperature, rapidly at first and then rises slowly to a maximum at absolute zero (Figure 1.1.)

Ferromagnets are also characterized by the phenomenon of hysteresis. In thermally demagnetized samples, the magnetization curve starts at the origin O (Figure 1.2.), and the magnetization M increases along $OABC$ when an external field H is applied. The magnetization saturates at a high field H_m and this value is referred to as the saturation magnetization M_s. When the field is removed, the specimen remains magnetized with a remnant magnetization or remnance M_r. Energy supplied by a reverse field H_c, known as the coercive field, is required to reduce the magnetization to zero. This part of the hysteresis loop is called the demagnetizaion curve DE. The applied field can be increased

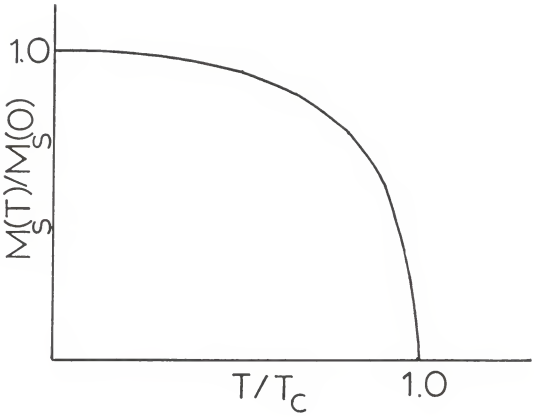

Figure 1.1. Variation of spontaneous magnetization with temperature.

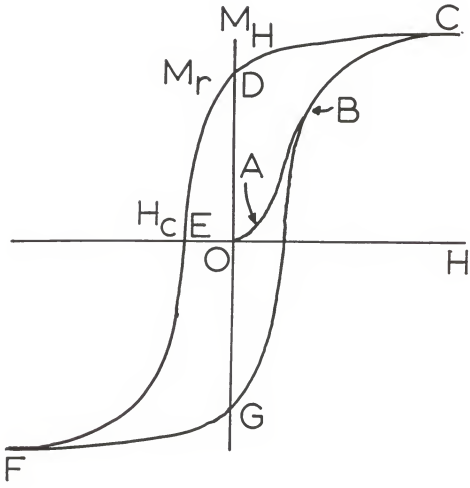

Figure 1.2. Magnetization Curve (OABC) and Hysteresis Loop (DEFGC)

further to again saturate the magnetization of the sample in the opposite direction (F) and the field when reduced to zero and again increased to saturate the magnetization in the original direction will complete the hysteresis loop.

Weiss[2] (1907), in order to account for the high intensity of magnetization in a ferromagnetic crystal at temperatures well below the Curie temperature T_c and in relatively low magnetic fields, postulated a large powerful internal *molecular* field proportional to the magnetization; it is now known that the origin of the molecular field lies in the quantum-mechanical exchange force. Thus, the strongly coupled atomic dipole moments which tend to be aligned parallel give rise to the spontaneous magnetization of ferromagnetic materials.

The exchange energy is given by:

$$E_{ex} = -J_{ex} \sum_{i,j} S_i S_j$$

where J_{ex} is the exchange integral which occurs in the calculation of the exchange effect, and S_i and S_j are the spin of electrons. If J_{ex} is positive, the exchange energy is a minimum when the spins are parallel, and a maximum when they are anti-parallel. This equation is summed over all atoms pairs in a crystal in order to determine the exchange energy.

1.3. Domains

It is also well known that a ferromagnetic specimen may also have no magnetic moment in a zero applied field. Weiss explained this difficulty by making

the assumption that specimens are composed of a number of small regions called domains, within each of which the local magnetization is saturated. The boundary region between two domains is called a domain wall. The domains present in a crystal serve to reduce the demagnetization energy associated with it. The dimensions of the domains can be calculated by minimizing the total free energy E_T, which may be written as the sum of several free energy terms[1]:

$$E_T = E_H + E_{MS} + E_K + E_\sigma + E_{ex} + E_O \tag{1.1}$$

Here E_H is the energy of the specimen's magnetization in the applied field H, E_{MS} is the magnetostatic energy, the self-energy, or the energy of the magnet in its own field, E_K is the crystalline anisotropy energy which arises from the fact that it is easier to magnetize a crystal in certain crystal directions called *easy directions* than other directions; E_σ is the magnetostrictive energy, E_{ex} is the exchange energy, and E_O is any other contribution to the free energy which may be present.

The domain wall serves as a transition layer between regions magnetized in different directions. This transition is not an abrupt change but a gradual one, since a wider wall involves less exchange energy. The width of the wall is then determined by the competition between E_{ex} and E_K, if we assume $E_D = 0$. Calculations[1] for a 180° wall in an uniaxial crystal have a wall width given by

$$\delta = \sqrt{\frac{J_{ex} S^2 \pi^2}{K \alpha}} \tag{1.2}$$

where J_{ez} is the exchange integral, K is the anisotropy constant, and α is the interatomic distance. The smaller the anisotropy, the thicker the wall; therefore, wall thickness increases with temperature because K almost always decreases with rising temperature. The wall energy per unit area is

$$\gamma = 2\pi\sqrt{\frac{J_{ez}S^2K}{\alpha}} = 2K\delta. \tag{1.3}$$

1.4. Theories of Coercivity

Theories used to explain coercivity are based on the irreversible movement of domain walls or irreversible rotation of the magnetization vector that give rise to the coercivity. Though in most real materials, more than one magnetization reversal mechanism is in effect it is of importance to review the major magnetic hysteresis models which follow.

1.4.1. Single Domain Particles

In order to reduce a magnetic samples magnetostatic energy it will spontaneously break up into several domains. When a specimen is very small, the exchange forces dominate, so that the particle is uniformly magnetized. This is in spite of the demagnetization energy and in the absence of an external applied field. The particle is then a single domain. For uniaxial materials the critical size L_c for a sample to be a single domain is given as[1]

$$L_c = \frac{1.7\gamma}{\pi^2 M_s^2}. \tag{1.4}$$

Now if we consider a spherical particle with negligible self (E_{MS}) and strain (E_σ) energy, the magnetization M will lie in the plane defined by the directions of the field and the polar axis where the angle between M and c is θ. The applied field, H, makes an angle α with the polar axis (Figure 1.3.).

The anisotropy energy is given by

$$E_K = K sin^2\theta \tag{1.5}$$

where θ is the angle between M and the polar axis. The energy in the applied field is

$$E_H = -HM_s cos(\alpha - \theta). \tag{1.6}$$

Thus, the total energy is

$$E_T = E_K + E_H = K sin^2\theta - HM_s cos(\alpha - \theta). \tag{1.7}$$

A minimum in the energy E_T corresponds to a stable position of the magnetization vector which will be along the direction the particle is magnetized. When E_T is a minimum we have

$$\frac{dE_T}{d\theta} = 0$$

$$\frac{d^2E_T}{d\theta^2} > 0$$

leading to,

$$\frac{1}{2} sin2\theta + h sin(\alpha - \theta) = 0 \tag{1.8}$$

where,

$$h = \frac{HM_s}{2K}. \tag{1.9}$$

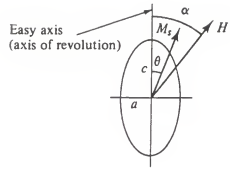

(a)

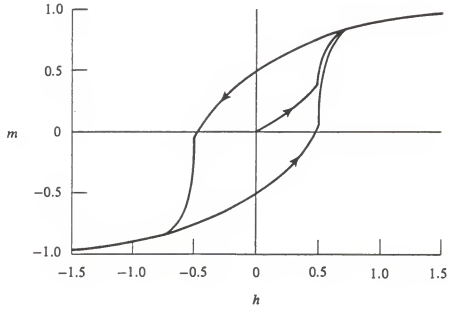

(b)

Figure 1.3. a) single domain particle in a magnetic field, H (Cullity[1]), b) hysterisis loop of an assembly of single domain non interacting particles (Stoner and Wolfarth[7]).

Here (1.8) gives the hysteresis loop of a single-domain particle with uniaxial anisotropy in a reduced field h and θ, and α. Thus the maximum coercive force occurs where h=1 and

$$H = \frac{2K}{M}.$$

For an array of spherical single domain particles randomly oriented and non-interacting, the coercive force is [2]

$$H_c = \frac{0.96K}{M_s}. \tag{1.10}$$

1.4.2. Domain Nucleation

Brown[8] showed that the field required to reverse the magnetization of a perfect crystal is given by

$$H_c = \frac{2K}{M_s}. \tag{1.11}$$

But in actual crystals the coercivity is much less than in (1.11). The calculation by Brown is one based upon a perfect crystal in the form of a perfect spheroid. Real crystals contain imperfections and irregular shapes. Interior imperfections include such defects as dislocations, interstitials, solute atoms, and vacancies. The shape of crystals may not only depart from spherical but may also have many surface irregularities. The condition for wall nucleation is that [1]

$$H_a + H_d > \frac{2K}{M_s} \tag{1.12}$$

where H_a is the applied field, and H_d is the demagnetization field at the nucleation position. The applied field required is much less than expected if H_d or M_s is larger

than normal, or if K is smaller than normal. The value of M_s is determined by the magnetic moment per atom and the exchange coupling among atoms and may vary in the vicinity of vacancies, interstitials, and dislocation where the strains are very large. The local value of K may also vary due to changes by imperfections or inhomogeneities in the particle which vary the spin-orbit coupling. But, the local variations in H_d are thought to play the prominent role in the nucleation of reversed domains. Thus, this theory indicates the coercivity is *decreased* by inclusions which make reversal easy.

1.4.3. Domain Pinning

This simple model can show how various parts of the hysteresis curve is related to domain wall movements. In a material, crystal imperfections hinder or *pin* the easy rotation of the domain wall. These hinderances are inclusions, microstresses, precipitates and any other inhomogeneities. To see how these effect domain wall movement, consider a 180° wall that lies parallel to the y, z plane and moves in the x direction when a field is applied. The wall energy or interaction energy is E_{wt} coming from a unit area of one wall located at a certain position(Figure 1.4.). Now, when the field is zero, the wall will lie at an energy minimum, but when a field is applied, the equilibrium position of the domain wall is given by

$$-2M_s H = \frac{dE_{wt}}{dx}, \tag{1.13}$$

from which we can find

$$H_c = \frac{1}{2M_s}\frac{dE_{wt}}{dx}_{max}. \tag{1.14}$$

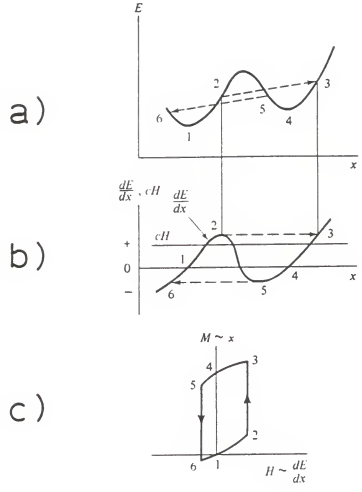

Figure 1.4. a) variation of interaction energy (E_{wt}) with x (Cullity[1]), b) the gradiant of the energy, along with line cH representing the pressure of the field on the wall (Cullity[1]), c) hysteresis loop from this model, because wall motion x is equivalent to change in magnetization M and $\frac{dE_{wt}}{dx}$ is proportional to H (Cullity[1]).

This gives a qualitative result from which the physical significance can be understood. The coercive force is a measure of the field required to move the domain wall past energy barriers and thus depends upon the maximum wall energy. The remnance of a material is then the result of a wall being taken from one energy minimum to the other by the application and removal of an applied field. Thus, from the domain pinning model we can say that imperfections in a real crystal, magnetic or otherwise, impede domain wall motion and *increase* the coercivity.

1.5. Permanent Magnets

The wide variety of magnetic materials can be divided into two groups, magnetically hard † and the magnetically soft ‡. A hard magnetic material is one which has an intrinsic coercivity of, say above 100Oe.

In order for a material to serve as a permanent magnet, two requirements must be met and a third is often quite desirable: a large value of remnance and coercivity are necessary and a high Curie temperature is also necessary in many applications. It is also essential to consider the B versus H curve, where B is the flux density, in analyzing the performance of a magnet. The (BH) product, commonly referred to as the energy product is found from the demagnetization curve of the material. Thus, permanent magnets are designed to operate in such a manner that the energy product is a maximum. Having $(BH)_{max}$ as large as possible allows the magnets to be made as small as possible.

† hard to magnetize and demagnetize
‡ easy to magnetize and demagnetize

CHAPTER 2

PREVIOUS AND PRESENT WORK ON RARE-EARTH TRANSITION-METAL INTERMETALLICS

2.1. Introduction to R-Fe-Intermetallics

The discovery [3,9] of the permanent magnet material $Nd_2Fe_{14}B$ has drawn attention to the possibility of finding other useful materials by exploring ternary intermetallic compounds. Some compounds like $R(Fe_{1-x}Al_x)_{13}$ were found to be cubic, and thus less attractive for permanent magnet applications [10,11]. Other materials considered have had similar problems such as low magnetic ordering temperatures or low crystal anisotropy.

Another approach has been to form a pseudobinary compound and adjusting its magnetic properties by gradually substituting a third component for one of the components in the binary parent material. A promising candidate seems to be $NdMn_{12}$ which has a uniaxial crystal structure (tetragonal $ThMn_{12}$ structure), but the Mn sublattice has virtually zero magnetization owing to the antiferromagnetic coupling within this sublattice [12]. Other attempts have been made to break this antiferromagnetic coupling by replacing Mn by other transition elements. These attempts were not successful since Curie temperatures for most cases were too low for practical purposes [13].

Present investigations [14~24] have addressed the problem of finding a suitable

compound of the $ThMn_{12}$ structure by abandoning the principle of substitution. New work has involved forming a ternary compound of the $ThMn_{12}$ type structure with iron and rare earth elements combined with small amounts of vanadium, chromium, titanium, molybdenum, tungsten, silicon or aluminum †. Buschow *etal*[17] first investigated $RFe_{10}V_2$ (R = rare earth-excluding the elements Pm, Er, and Yb) in bulk samples.

In the investigations of this new class of magnetic materials, Buschow *etal* found the $ThMn_{12}$ type structure for all R excepting $R = La$ and Pr. Indexing was done according to a tetragonal unit cell with lattice constants $a = 851.7pm$ and $c = 477.4pm$ in the Gd containing sample and found to be of the 1:12 type structure. The Fe and V atoms were found to be statistically distributed over the three Mn positions. The crystal structure is schematically represented in Figure 2.1. Since the x-ray atomic scattering factors of the V and Fe atoms are similar, neutron diffraction studies were done[20] so that conclusions regarding the site occupation preferance of $V(Fe)$ over the 8(i), 8(j), and 8(f) sites in the underlying crystal structure could be made. Fits were made to experimental data for $YFe_{10}V_2$ with preferential sites of the vanadium atoms determined to be almost exclusively the 8(i) site. Similar work has also been done for an $Gd_8Fe_{10}Mo_2$ sample.

The occurrence of the $ThMn_{12}$ type compounds is not limited to the exact

† For aluminumum containing samples the 1:12 phase forms in crystallized ribbon samples only[14].

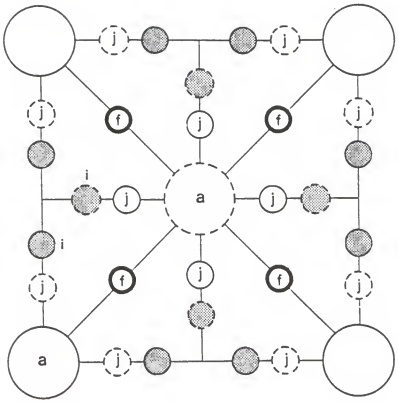

Figure 2.1. Basal plane projection of $ThMn_{12}$ unit cell. Rare earth atoms (large circles) on sites (2a) and the atoms on the sites 8(i) and 8(j) are located in the planes $z = 0$ (full symbols) or $z = \frac{1}{2}$ (dashed symbols). Atoms on the sites 8(f) reside in the planes $z = \frac{1}{4}$ and $z = \frac{3}{4}$. The 8(i) atoms are indicated by shaded spheres. Sites 8(i), 8(j), and 8(f) are the $Fe(T)$ atoms where $T = Ti, V$, and Mo (from Buschow *etal*).

composition $RFe_{10}T_2$ where $T = V, Cr, Ti, Mo, W, Si$, or Al. The most extensive solid solution ranges of $RFe_{12-x}T_x$ are observed in the systems containing V where the range extends from $x = 1.4$ to 3.5[17]. For the Si and Mo compounds the solid solution ranges are much smaller and for $T = Ti$ and W the $ThMn_{12}$ structure is observed for $x = 1.2$[17]. Some structural and magnetic data of various ternare Fe rich rare earth compounds and related compounds is given in Table 2.1., summarized by Buschow *etal.*

Extensive investigations of lattice constants, Curie temperatures, and determination of the anisotropy fields of these materials has been done in bulk samples. It has been found that these materials follow the usual ferromagnetic coupling with light rare-earths and transition metals and an antiferromagnetic coupling with heavy rare-earths and transition metals. The Curie temperatures are almost similar to those found in the 2:14:1 materials, and vary with the R component approximately according to the de Gennes factor

$$G = (g-1)^2 J(J+1), \tag{2.1}$$

the lowest and highest T_c values observed for $R = Lu$ and $R = Gd$, respectively[17]. High field magnetization measurements made on several samples have shown and Fe sublattice anisotropy field of $H_A = 40kOe$[16,19].

2.2. Present Work

Previous work on these alloys has been done on bulk samples. The purpose of this investigation is to prepare mostly ribbon samples having the $ThMn_{12}$

Table 2.1. Structural and magnetic data found in summary from Buschow *etal*[21].

compound	structure	T_c(Y)	T_c(Gd)	A^0_2	3d sublattice anisotropy
$R_2Fe_{14}B$	$Nd_2Fe_{14}B$	571	660	+680; + 661	easy axis
$R_2Fe_{14}C$	$Nd_2Fe_{14}B$	495*	620	+714; + 586	easy axis
$R_2Co_{14}B$	$Nd_2Fe_{14}B$	1010	1053	+580; + 406	easy plane
$RFe_{10}V_2$	$ThMn_{12}$	532	616	-140	easy axis
$RFe_{10}Cr_2$	$ThMn_{12}$	515	580	--	easy axis
$RFe_{10}Mo_2$	$ThMn_{12}$	350	400	-120	easy axis
$RFe_{10.8}W_{1.2}$	$ThMn_{12}$	500	570	--	easy axis
$RFe_{10.8}Ti_{1.2}$	$ThMn_{12}$	520	600	--	easy axis
$RFe_{10}Si_2$	$ThMn_{12}$	530	610	-120	easy axis
RFe_9Ti_2	$CeMn_6Ni_5$	--	280	--	--
R_2Fe_{17}	Th_2Ni_{17}	324	476	- 70; + 70	easy plane
R_2Co_{17}	Th_2Ni_{17}	1186	1218	-120; - 50	easy plane
RCo_5	$CaCu_5$	987	1014	-698	easy axis
RFe_4B	$CeCo_4B$	573*	--	-775; -1221	easy axis
$RCo_{12}B_6$	$SrNi_{12}B_6$	156	163	--	--

type structure and to investigate the magnetic and structural properties with a particular emphasis on magnetic hysteresis.

Apparently, this system of compounds generally has a relatively high magnetization due to the high iron content, and has Curie temperatures which are relatively high and comparable to the 2:14:1 magnet materials. Anisotropy[16,19] constants of the iron sublattice are also found to be comparable to the 2:14:1 magnets.

Some preliminary investigations have shown that samples prepared using rapid quenching techniques may lead to good hard magnetic properties[22,23,24]. It is hoped that by using the melt-spinning technique that we may find good hard magnetic properties in crystallized ribbons and that these materials may prove to be good canidates for permanent magnet developement.

CHAPTER 3

EXPERIMENTAL

3.1. Sample Preperation

The samples were prepared from 99.9% pure materials by means of arc-melting in purified argon. The ternary R-Fe-T alloys were remelted four times for high homogeneity. Weight losses of samples after melting were kept under 0.5% .

Amorphous or microcrystalline alloys were prepared by the melt-spun technique (Figure 3.1.). Small portions of the as-cast alloy ingots were placed in a quartz tube. Each tube had a small orifice (< 0.5mm) through which the molten alloy could be ejected onto the surface of a variable speed, rotating copper wheel. The top of the quartz tube was connected to a pressurized Ar gas cylinder. An induction coil surrounded the tube and the alloy to be melt-spun. An Ar atmosphere was used in the melt-spinning chamber by evacuating the chamber several times and flushing with high purity Ar gas. The coil when activated would melt the pieces of alloy into a fluid mass. Pressurized argon gas was then introduced into the top of the quartz tube. This then ejected the molten alloy through the opening at a constant rate onto the rotating copper wheel (7000 rpm). The orifice was located approximately 1-2mm from the rotating disk, and an estimated cooling rate of 10^6K/s is obtained which produced ribbons 1-3mm wide and 20-60 micron thick.

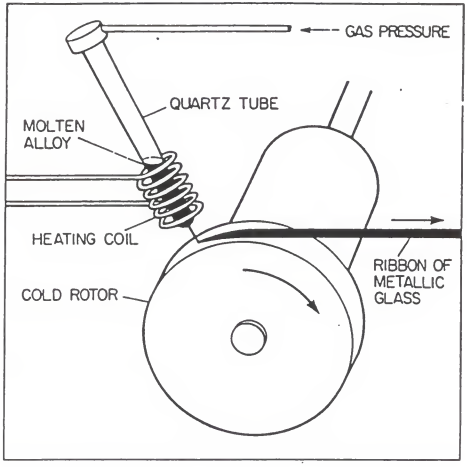

Figure 3.1. The melt-spinning apparatus.

3.2. Crystallization

The crystalization temperature of the as-spun samples was found using a Dupont model 901 differential scanning calorimeter (DSC). A small portion of ribbons was used, and as the temperature was increased to a desired value, the DSC system measures the differential energy needed to keep both the sample and reference channels at the same temperature throughout the analysis. Thus, when the sample crystallizes it reaches a more ordered state which usually involves an exothermic process, and the heat release or apparent heat capacity is detected which corresponds to the crystallization temperature of the amorphous sample. This process was important in determining the temperature which ribbon samples needed to be heat-treated at in order to crystallize or grow the 1:12-type phase. The ribbon samples were then heat-treated at the crystallization temperature found using the DSC.

As-cast samples were also heat-treated in order to obtain a single phase. The as-cast ingot were homogonized in evacuated quartz tubes at 900-1100$^{\circ}C$ from two to four days.

3.3. Magnetic Measurements

Hysteresis loops were measured using a low field vibration sample magnetometer (VSM) with fields up to 17kOe. Loops were taken before and after crystallization. A SQUID (superconducting quantum interference device) was used to

provide further magnetic sample characterization of the sample for temperatures ranging from $1.7K$ to $400K$ and for fields ranging up to 55kOe.

Thermomagnetic data was obtained, giving the temperature dependence of M from room temperature up to 750°C. This gave information as to the magnetic phases present above room temperature and their transition temperatures. These measurements are taken using a low applied field of about 300Oe which is kept constant during the experiment ($M_H(T)$). The samples were wrapped in tantalum foil and an argon atmosphere was present to prevent oxidation. The temperature was then increased slowly to a desired value and then subsequently decreased and from kinks in the $M_H(T)$ curve, the Curie temperature can be found.

Ac susceptibility (χ_{ac}) measurements were also taken of samples which showed only one magnetic phase above room temperature. These measurements provide more information about magnetic phase transitions from room temperature down to $4.2K$. The susceptibility of the sample is measured as a function of temperature in the presence of an alternating low magnetic field of 1.8kOe.

3.4. Crystal Structure and Microstructure Studies

Studies of the crystal structure were made in order to verify the presence of the $ThMn_{12}$ type phase in crystallized ribbon samples and other phases present in as-spun ribbons. In order to attempt to correlate the magnetic properties with the structural properties, microstructure studies were conducted on samples with optimum and lesser hard magnetic properties.

3.4.1. X-ray Diffraction

Both as-spun and crystallized ribbons were investigated. Samples were prepared for x-ray diffraction by finely grinding ribbons which had been crystallized until they were in a powderlike form. As-spun ribbons were examined by carefully mounting a piece of ribbon in the x-ray camera centered in the x-ray beam line. X-ray diffraction studies were made using $Cr_{K\alpha}$ radiation. The d-spacings determined from x-ray diffraction of crystallized ribbons were matched with those found previously[15] in as cast samples of the $ThMn_{12}$ type structure.

3.4.2. Transmission Electron Microscopy (TEM)

A JEOL 100C TEM was used to examine the microstructure of several selected samples. The samples were prepared by first crystallizing ribbons which had been wrapped in tantalum foil by heat treating for a short period of time in an evacuated quartz tube. In order to produce a thin region (500-5000 Å) needed for TEM, the samples were ion thinned for twelve hours (Techniques MIM IV-C Ion Thinner).

Analysis involved selected area diffraction (SAD) which gives a two dimensional array of rings, each ring corresponding to a particular set of reflecting planes. SAD was used to determine all metallurgical phases which precipitate and other microstructure features of samples. Bright field (BF) and dark field (DF) techniques were also employed to determine grain size and orientation as well as the distribution of all phases present in the sample.

The chemical composition of the phases present in the samples was determined by using an energy dispersive analysis (EDXA) with the TEM. A spatial resolution of 0.04microns is available.

Lorentz electron microscopy was also employed in order to observe magnetic domains and domain wall structure. The *Fresnel Method* and *Foucalt Technique*[25] can be used in order to observe domain structure.

CHAPTER 4

RESULTS AND DISCUSSION

4.1. Introduction

This chapter will contain the structural and magnetic properties of the 1:12 type phase samples studied. The magnetic measurements will be given first followed by the microstructure. A comparison will be made of the structural properties of the samples with the magnetic properties in order to correlate the magnetic and structural results. This chapter will be followed by a conclusion in which the ideas and results presented here will be tied together.

4.2. Crystallization Studies

Ribbon samples were annealed at about 700°C. The annealing temperature was determined by differential scanning calorimetry (DSC) which showed an exothermic peak (related to crystallization) at about 650°C (Figure 4.1.). This annealing temperature crystallized amorphous ribbons, and was also used on microcrystalline ribbons to ensure there crystallinity. Slightly lower and higher annealing temperatures were also used in order to optimize the magnetic properties of the samples.

In order to find a single phase in as-cast alloys, the samples were homogenized from two to four days at temperatures around 900-1100°C. This heat treatment failed to produce single phase alloys in most cases. Most homogonized samples

had α-Fe and other secondary phases present. However, the single major phase present in the alloys studied was the $ThMn_{12}$-type phase.

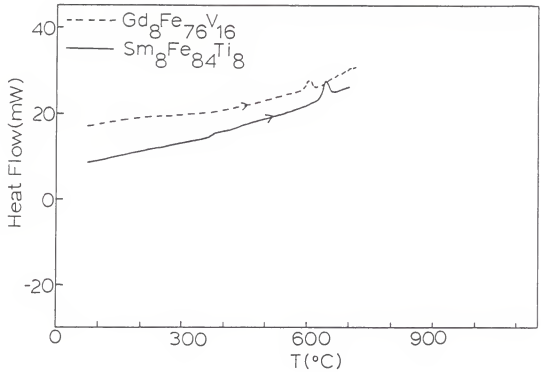

Figure 4.1. DSC data for $Sm_8Fe_{84}Ti_8$ and $Gd_8Fe_{76}V_{16}$ ribbon samples showing peaks at the crystallization temperature of each sample.

4.3. Magnetic Properties

In this study, three elements $T = Ti, V$, and Mo were used together with rare earths R and $Fe(Co)$ in R-$Fe(Co)$-T to form the $ThMn_{12}$ type compounds. The following samples were made:

$R_8(Fe, Co)_{84}Ti_8$ where $R = Y, Sm, Nd, Gd$ and Dy

and,

$R_8Fe_{92-x}V_x$ where $x = 8, 16$ and $R = Y, Sm, Nd$, and Gd

and,

$R_8Fe_{76}Mo_{16}$ where $R = Sm, Nd$,and Gd.

4.3.1. Hysteresis Loops

Hysteresis loops were taken at room temperature. As-cast and homogonized samples had negligible coercivities of about $100Oe$ with a maximum of $750Oe$ in the $Sm_8Fe_{84}Ti_8$ sample (Table 4.1., 4.2., and 4,3.). After heat homogonizing samples showed little change in coercivity. Low coercivities have been characterisitic of the 1:12 type samples and thus ribbon samples were also studied in hopes of finding higher coercivities. This was expected because of the much smaller grain sizes found in ribbon samples. The as-spun samples were either amorphous or microcrystalline †.

† This is confirmed by x-ray diffraction, $M_H(T)$ measurements, and from DSC results.

Hysteresis loops of as-spun Ti containing ribbon samples, which were amorphous, show low coercivities (Figure 4.2.), as did all ribbons which were amorphous. After crystallization, the coercivity increases, and in most cases it is significantly larger than in the as-cast or homogonized samples (Figure 4.2. and 4.3. and Table 4.1., 4.2. and 4.3.) The hysteresis loops in all samples studied do not appear to be saturated. In Figure 4.2. a slight asymmetry about the M axis may be seen because the magnetization of the sample was not saturated. For the Ti containing samples, the magnetization of the as-spun ribbons is lower than in the crystallized ribbons, (Figure 4.2. and Table 4.1.). This is most likely due to the variation in the local exchange environment when comparing the amorphous and crystalline state and in some cases to the presence of α-Fe in the crystallized ribbons. The samples containing Mo or V did not show this behavior, but were not amorphous in the as-spun state. All crystallized ribbons had a saturation magnetization approximately equal to their as-cast and homogonized counterparts. The constricted shape of the hysteresis loop in Figure 4.3. indicates that more than one magnetic phase is present in this sample. This behavior was also seen in other samples containing Mo or V.

The coercivity was found to be strongly temperature dependent indicating a strong thermal activation process. In Figure 4.4. the coercivity of $Sm_8Fe_{84}Ti_8$ increases from 2kOe to about 6kOe at $300K$ and $10K$ respectively. The Sm containing samples showed the highest coercivities. This is consistent with the anisotropy data of Buschow which showed an easy axis for the Sm-Fe-V samples

with an anisotropy field of approximately $150kOe$. The Nd containing compounds have an easy plane and this would justify the much lower coercivities obtained in these systems. The coercivities found in these compounds are much lower than those obtained in $R_2Fe_{14}B$ alloys despite having anisotropy fields which are comparable in magnitude. The low coercivities can be explained by the large amount of α-Fe which is found in all of the samples after crystallization. α-Fe is a magnetically soft bcc phase which allows for easy domain wall motion. Small amounts of α-Fe have been seen to dramatically decrease the hard magnetic properties in other systems. Thus, it is necessary to reduce the amount of α-Fe in these samples by varying the composition, changing the heat treatment of the sample, or by some other processing technique.

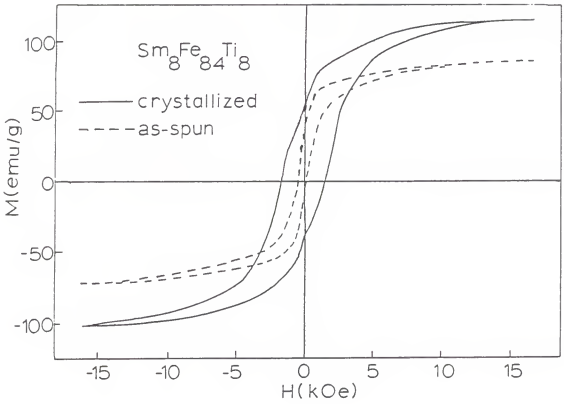

Figure 4.2. Hysteresis loops of as-spun and crystallized $Sm_8Fe_{84}Ti_8$ ribbon sample.

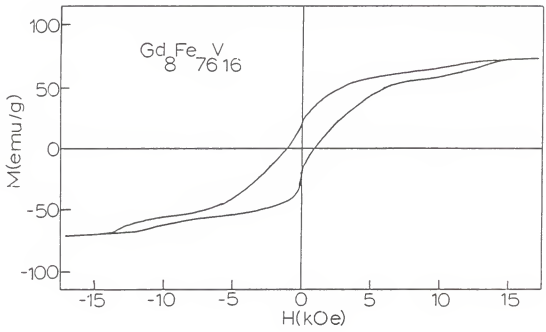

Figure 4.3. Hysteresis loop of a $Gd_8Fe_{76}V_{16}$ ribbon sample.

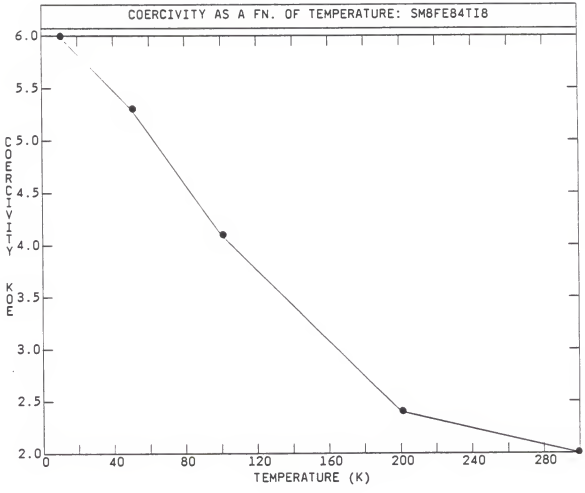

Figure 4.4. Coercivity as a function of temperature ($H_c(T)$) for $Sm_8Fe_{84}Ti_8$ crystallized ribbon sample.

Table 4.1. Magnetic data from titanium containing samples.

* indicates T_c of secondary phase.

R=	$T_c(°C) \pm 5°$	$M_s(emu/g)$	$H_c(Oe)$
	As-cast $R_8Fe_{84}Ti_8$		
Y	255	116	200
Nd	275	126	100
Sm	307	123	200
Gd	337	71	400
Dy	271	79	200
	Homogonized $R_8Fe_{84}Ti_8$		
Y	248	105	100
Nd	145*,272	128	100
Sm	187*,303	122	750
Gd	337	74	400
Dy	257	74	200
	As-spun amorphous ribbons $R_8Fe_{84}Ti_8$		
Y	40	49	100
Nd	40	75	100
Sm	44	84	100
Gd	105	72	100
Dy	40	36	200
	Crystallized ribbons $R_8Fe_{84}Ti_8$		
Y	212	112	400
Nd	210	116	500
Sm	254	114	2000
Gd	296	94	1100
Dy	210	78	600

Table 4.2. Magnetic data from vanadium containing samples.
* indicates T_c of secondary phase.

R=	$T_c(°C) \pm 5°$	$M_s(emu/g)$	$H_c(Oe)$
	As-cast $R_8Fe_{84}V_8$		
Y	153*,285	115	100
Nd	170*,346	140	100
Sm	210*,410	92	500
Gd	275*,387	80	100
Dy	185*,380	80	100
	Homogonized $R_8Fe_{84}V_8$		
Y	195*,304	128	100
Nd	164*,346	147	100
Sm	180*,410	164	500
Gd	272*,387	82	400
Dy	314	80	200
	Crystallized Ribbons $R_8Fe_{84}V_8$		
Nd	351	146	750
Dy	326	87	1000
	As Cast $R_8Fe_{76}V_{16}$		
Y	–	90	100
Nd	–	133	100
Sm	–	95	400
Gd	–	88	100
	Crystallized Ribbons $R_8Fe_{76}V_{16}$		
Y	259	92	900
Nd	267	125	200
Sm	360	90	1500
Gd	342	72	1000

Table 4.3. Magnetic data from molybdemum containing samples.

R=	$T_c(°C) \pm 5°$	$M_s(emu/g)$	$H_c(Oe)$
	As-cast $R_8Fe_{76}Mo_{16}$		
Y	66	37	100
Sm	–	90	300
Gd	–	45	100
	Crystallized ribbons $R_8Fe_{76}Mo_{16}$		
Y	60	22	500
Sm	239	78	750
Gd	133	44	750

4.3.2. Thermomagnetic Measurements ($M_H(T)$)

Thermomagnetic data were used to determine the magnetic transitions present in the samples. The Curie temperatures (T_c) were found by extrapolating the steepest part of the $M_H(T)$ curve to zero. Figure 4.5. is the $Sm_8Fe_{84}Ti_8$ sample which shows T_c of the as-cast and homogonized samples to be about 305°C. The ribbon sample is initially amorphous and has an amorphous Curie temperature (T_c^{am}) of 70°C. The sample is then heated above the crystallization temperature (found using the DSC (Figure 4.1.)) and cooled to room temperature where T_c of the 1:12 phase is 255°C. The magnetization is not equal to zero at temperatures above the T_c of the $ThMn_{12}$ type phase, indicating the presence of another phase which is found to be α-Fe †. Thermomagnetic data for $R_8Fe_{76}V_{16}$ ribbon samples are shown in Figure 4.6. A summary of Curie temperatures obtained are given in Tables 4.1., 4.2. and 4.3. They behave quite analogously to the $R_2Fe_{14}B$ compounds with T_c increasing up to Gd, which gives the highest value and then decreasing for heavier rare earths, which is commonly seen in rare earth metals and their compounds.

In Ti containing samples, the Curie temperatures were found to be lower in crystallized ribbon samples than in as-cast or homogonized samples. In V or Mo containing samples the T_c was nearly the same for bulk and ribbon samples. The T_c of V samples was found to increase with increasing Fe concentration (Table 4.2.) which agrees with results by Buschow *etal*. Energy dispersive x-ray analysis

† Confirmed by x-ray and electron diffraction.

(EDXA) was used to further investigate the composition of some samples, and it was found that the bulk samples had a composition approximately the same as that of the starting materials. The crystallized ribbon samples studied, however, showed a slightly lower Sm and Fe concentration than was found in the as-cast or homogonized samples. The lower Sm concentrations in the ribbon samples are related to rare-earth losses during melt spinning. The differences in chemical composition are very small between the bulk and ribbon samples and probably have an insignificant effect on the Curie temperature. On the other hand $M_H(T)$ and microstructure data showed the presence of Fe in the form of α-Fe in the samples. It is also true that the technique used allows for a spatial resolution of 0.1microns which was larger than the single crystal size (150-800Å) of the samples studied. Thus, the composition found using EDXA is an average over a relatively large region of the sample which could contain several α-Fe crystals along with the 1:12 type phase. This would make the sample appear to have a greater amount of Fe present in the 1:12 structure, which according to detailed studies by Buschow would cause us to expect a higher Curie temperature than found in Ti containing ribbon samples. Similar $M_H(T)$ results were also observed for samples containing V or Mo.

Another possibility of low T_c in Ti containing ribons is that the site occupation of the Ti atoms may be different in the ribbon samples than in the bulk samples. This would cause the Curie temperature to be different since the T_c is dependent upon the local exchange interactions of the constituent atoms in the

sample. In Ti containing alloys it appears that the site occupation of Ti atoms in the 1:12 structure is different when the sample is crystallized from the amorphous phase than when is is made directly microcrystalline from the melt. The V or Mo containing ribbons were microcrystalline in the as-spun state and had Curie temperatures approximately equal to their bulk counterparts. This idea was tested by varying the wheel speed when making Ti containing ribbons for a $Sm_8Fe_{84}Ti_8$ sample. By using slower wheel speeds microcrystalline ribbons were formed. Thermomagnetic measurements ($M_H(T)$) confirmed the microcrystallinity of the ribbons which had a Curie temperature of 310℃ compared to 254℃ found previously in crystallized amorphous ribbons. Also a slight transition at a lower temperature was observed equal to the T_C found in crystallized amorphous ribbons, which indicates that a small portion of ribbon may have been amorphous and then crystallized during heating. The fact that the T_c was near the value found in bulk samples in the microcrystalline ribbons supports the idea that the site occupation of the Fe and Ti atoms may be different in samples which were amorphous and then crystallized. Mössbauer spectroscopy or neutron diffraction studies are necessary to confirm the site occupations in the two types of ribbons.

χ_{ac} showed that the crystallized ribbons studied had no magnetic phase transitions from room temperature to $77K$. An $M_R(T)$ from room temperature to $10K$ showed no transitions in a crystallized $Sm_8Fe_{84}Ti_8$ ribbon sample (Figure 4.7.).

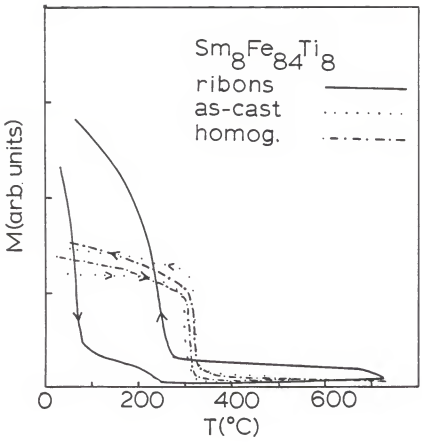

Figure 4.5. Thermomagnetic data for $Sm_8Fe_{84}Ti_8$ samples.

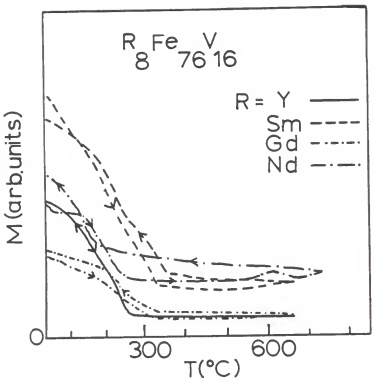

Figure 4.6. Thermomagnetic data for $R_8Fe_{76}V_{16}$ ribbon samples where $R = Y, Sm, Nd$, and Gd.

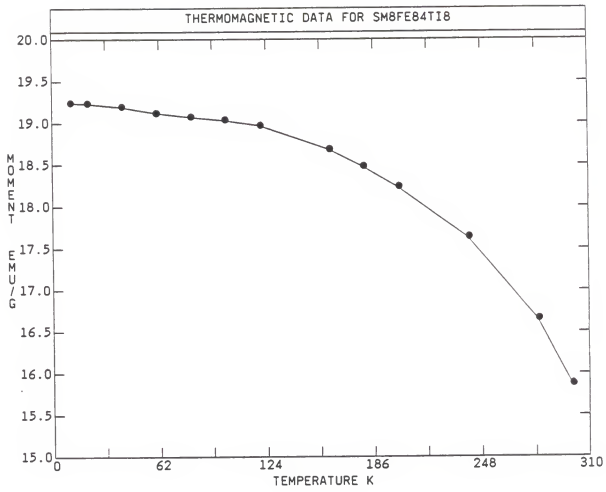

Figure 4.7. Remnance data for a $Sm_8Fe_{84}Ti_8$ crystallized ribbon sample below room temperature.

4.3.3. Effect of Cobalt Substitution

In this section, the effect of replacing iron with cobalt will be discussed. *Nd-Fe-Ti* samples were primarily investigated. Most of the compounds prepared were composed of several phases with the $ThMn_{12}$ type phase as the primary phase present. The presence of secondary phases in homogonized samples indicated that the compound exists in a definate atomic ratio of the elements present, and allows for little variation in the compostion range.

In Table 4.4. the Curie temperature of ribbon samples can be seen to increase with increasing cobalt content, and then decreasing somewhat for samples containing no iron. Saturation values of magnetization can also be seen in Table 4.4. where there is a slight decrease in magnetization in the sample containing no iron. Again, a slight increase in coercivity is found in ribbon samples. The thermomagnetic data for the *Nd-(Fe, Co)-Ti* samples is shown in Figure 4.8.

Ac susceptibility studies on Co-substituted samples showed no additional magnetic transitions in the crystallized ribbons below room temperature down to $77K$. However, in as-spun ribbons a small peak occurs just below room temperature and at about $170K$ (Figure 4.9. for samples with cobalt substitution). Thermomagnetic measurements using the SQUID magnetometer for the as-spun and crystallized ribbons of $Nd_{8.3}\ Fe_{41.7}\ Co_{41.7}Ti_{8.3}$ showed a large change in magnetization beginning at about $120K$ (Figure 4.10) with the magnetization increasing with increasing temperature. This magnetic transition may be related

to spin reorientation. Hysteresis loops of alligned powders from the same sample below and above the transition temperature at $10K$ and $190K$ showed coercivities of 4.5 and 0.2kOe respectively. This large change in H_c is attributed to this transition. Hysteresis loops on alligned powders above and below the transition temperature and at various temperatures about the transition temperature have confirmed that this transition is due to spin reorientation. The sample studied was found to switch from an easy plane to and easy axis at temperatures below the transition. Mössbauer spectroscopy is needed for an accurate determination of this reorientation.

Table 4.4. Magnetic data from Nd-(Fe,Co)-Ti ribbon samples.
* indicates T_c of secondary phase.

type=	$T_c(°C) \pm 5°$	$M_s(emu/g)$	$H_c(Oe)$
	$Nd_8Fe_{84}Ti_8$		
as-cast	275	126	100
homogonized	272	128	100
cryst. ribbon	210	116	500
	$Nd_{8.3}Fe_{41.7}Co_{41.7}Ti_{8.3}$		
as-cast	720	129	100
homogonized	680	134	100
cryst. ribbon	600*,662	110	100
	$Nd_{8.3}Co_{83.4}Ti_{8.3}$		
as-cast	155*,722	92	200
homogonized	159*,675,752	88	200
cryst. ribbon	491	95	500

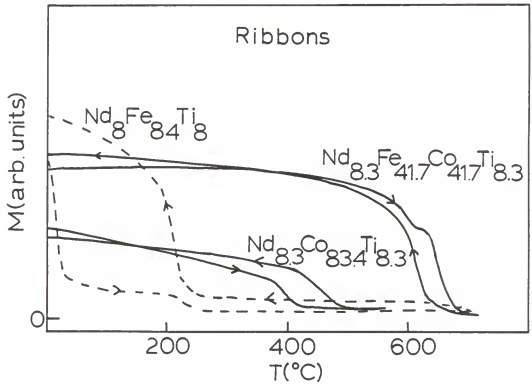

Figure 4.8. Thermomagnetic data for Nd-(Fe, Co)-Ti ribbon samples.

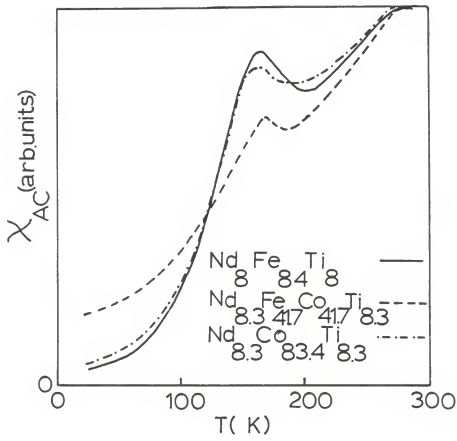

Figure 4.9. Ac susceptibility data for as-spun Nd-(Fe, Co)-Ti ribbon samples.

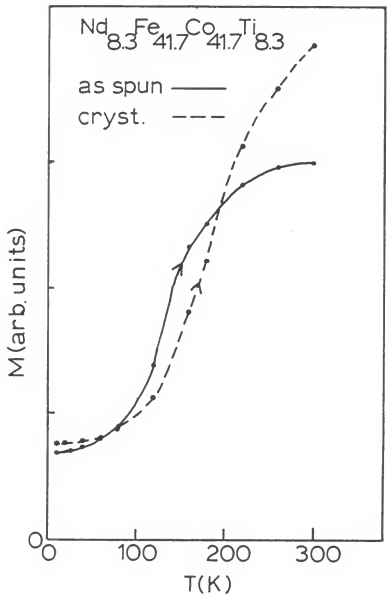

Figure 4.10. Low temperature thermomagnetic data ($M_H(T)$) for Nd-(Fe, Co)-Ti ribbon sample.

4.4. Crystal Structure and Microstructure Studies

X-ray diffraction studies in as-spun $R_8Fe_{84}Ti_8$ samples showed rather diffused rings which are characteristic of amorphous materials. The amorphousness was also comfirmed as previously mentioned by DSC (Figure 4.1.) and thermomagnetic measurements (Figure 4.5.). Samples containing V or Mo were microcrystalline in the as-spun state. Similar studies showed the presence of the $ThMn_{12}$ type phase in all crystallized ribbon samples. As-cast and homogonized samples also showed the presence of the 1:12 phase. A complete structural study of the as-cast and homogonized samples will not be presented here since this work has previously been reported[18]. A detailed analysis of the x-ray diffraction of $Sm_8Fe_{84}Ti_8$ was completed and diffraction lines were found to be in accordance with the $ThMn_{12}$ structure (Table 4.5.). The lattice parameters for the $Sm_8Fe_{84}Ti_8$ sample were found to be a = 8.589Åand c = 4.798Åwhich are close to those reported by Buschow *etal.* Visual inspection of x-ray diffraction obtained from crystallized samples of all other compositions made are isotypic and correspond to the previously mentioned type structures.

Further microstructure studies have been initiated on several ribbon samples using TEM. Selected area diffraction (SAD) also confirms the presence of the $ThMn_{12}$ type phase. Figure 4.11. shows a $Sm_8Fe_{84}Ti_8$ sample with lattice parameters a = 8.589Åand c = 4.798Å. Microstructure studies on annealed samples showed the presence of α-Fe and possibly a bcc Fe-T phase ($T = V, Mo,$ or Ti) as

also found by Buschow *etal* in samples with relatively low vanadium concentrations (Figure 4.12.). The presence of α-Fe and R-T have also been reported in other studies[17,22].

TEM studies show a fine grain structure (Figure 4.13.) with an average grain size of about 500Å. This grain size is similar to that observed in R-Fe-B alloys. Ribbon samples which were subjected to long heat treatments (greater than ten minutes) had much larger grain sizes 1000 to 2000Å(Figure 4.14.) and also had significantly lower coercivities which were only slightly higher than the as-spun amorphous samples, and were in some cases significantly lower than the as-spun microcrystalline samples (V or Mo containing samples). Lorentz microscope studies show domain walls along grain boundaries (Figure 4.15.).

Table 4.5. Observed and calculated diffraction angles and d spacings for $Sm_8 Fe_{84} Ti_8$ using $Cr_{K\alpha}$ radiation. The lattice parameters found are $a = 8.589$Åand $c = 4.798$Å†. The d-spacings are calculated based on the $ThMn_{12}$ structure with space group $I4/mmm$ (no. 139). The selection rules are as follows:

index	selection rule (n = integer)
hkl	$h + k + l = 2n$
$hk0$	$h + k = 2n$
$0kl$	$k + l = 2n$
001	$l = 2n$

† Buschow[18] has found $a = 8.561$Åand $c = 4.792$Åfor $SmFe_{10.8}Ti_{1.2}$

X-ray diffraction data for $Sm_8Fe_{84}Ti_8$

Observed		Calculated		
θ	$d(hkl)$(Å)	hkl	θ	$d(hkl)$(Å)
		101	15.860	4.1887
		220	22.153	3.0367
22.68	2.9708	211	22.458	2.9986
25.08	2.7024	310	22.933	2.7161
27.93	2.4456	022	28.510	2.3990
32.23	2.1474	400	32.228	2.1472
32.58	2.1273	321	32.421	2.1337
33.43	2.0793	202	33.144	2.0944
34.50	2.0244	330	34.446	2.0244
		420	36.600	1.9206
		411	36.871	1.9108
37.08	1.8999	222	37.467	1.8824
		510	42.828	1.6844
42.03	1.7109	431	45.075	1.6173
42.03	1.7109	501	45.075	1.6173
		332	47.741	1.5472
		440	48.953	1.5183
		521	49.164	1.5135
49.75	1.5009	422	49.796	1.4993
		213	50.856	1.4765
51.30	1.4678	530	51.022	1.4730
52.90	1.4362	600	53.123	1.4315
55.20	1.3950	303	55.097	1.3963
58.32	1.3461	611	57.709	1.3564
60.10	1.3210	323	59.584	1.3278
66.45	1.2960	532	65.815	1.2553
		631	67.764	1.2371
68.67	1.2297	602	68.671	1.2293
71.48	1.2081	550	70.152	1.2147
71.48	1.2081	710	70.152	1.2147
73.37	1.1955	004	72.677	1.1995
		640	74.026	1.1911

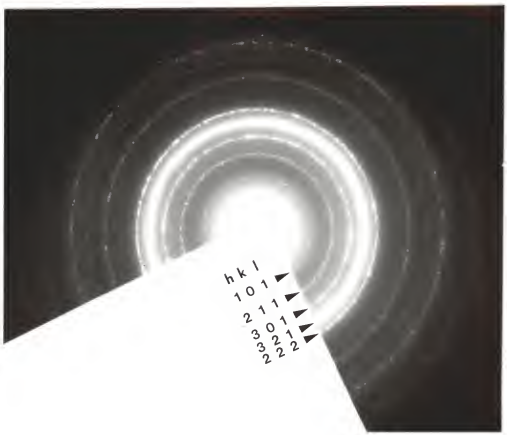

Figure 4.11. SAD of crystallized $Sm_8Fe_{84}Ti_8$ ribbon sample with lattice parameters a = 8.589Åand c = 4.798Å. This nearly pure $ThMn_{12}$ type phase was heat treated by $M_H(T)$ up to 700°C and has a coercivity of $2kOe$.

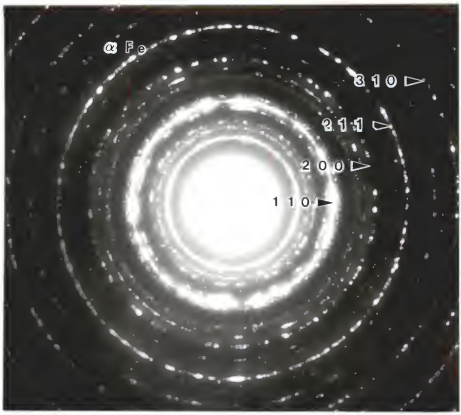

Figure 4.12. SAD of crystallized $Sm_8Fe_{84}Ti_8$ ribbon sample which was heat treated at 700$^{\circ}C$ for 15 minutes and has large amounts of α-Fe present. This sample had low coercivity.

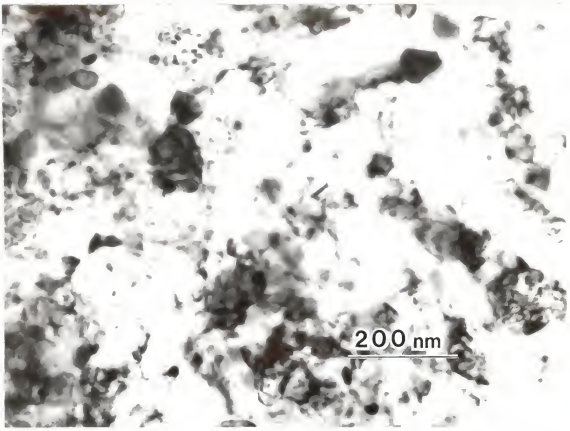

Figure 4.13. Microstructure of crystallized $Sm_8Fe_{84}Ti_8$ ribbon sample with an average grain size of 500Å.

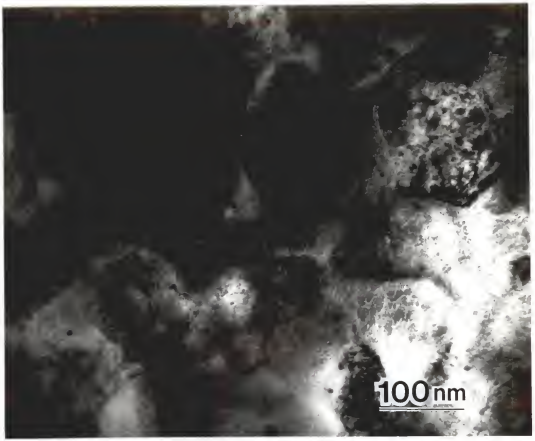

Figure 4.14. Sample subjected to the same heat treatment as Figure 4.10.b. with larger grains of 1000-2000Åand a low coercivity.

Figure 4.15. Magnetic domain walls in $Sm_8Fe_{84}Ti_8$ ribbon sample with H_c = $2kOe$.

CHAPTER 5

CONCLUSIONS

The 1:12 phase has been observed in all the as-cast, homogonized, and crystallized melt-spun samples studied. The various samples studied have shown some potential for permanent magnet developement. The saturation magnetization and Curie temperatures are sufficiently high and comparable to the 2:14:1 compounds. The alloys have the required uniaxial structure with the Fe sublattice having an anisotropy field of approximately 40 kOe and the Sm containing alloys having a high anisotropy of approximately 150kOe. The corrosion resistance of the alloys appears to be better than the 2:14:1 alloys (by visual inspection of as-cast and ribbon materials exposed to air for several months).

Of the samples studied, those containg Mo would appear to be the poorest canidates for permanent magnets since the Curie temperature and saturation magnetization of the samples are low when compared to the Ti or V containing samples. The most promising canidate for permanent magnet developement would be the Sm-Fe-$Ti(V)$ samples. These samples have sufficiently high T_c and M_s to be considered for permanent magnets. They also have a high anisotropy. If samples free of impurity phases could be produced, high coercivities could be found and these materials may be able to compete with the $Nd_2Fe_{14}B$ type magnets.

The bulk samples and crystallized ribbons behave similarly, with the T_c varying approximately according to the de Gennes factor. Both have values of M_s

which are nearly equal in each respective sample. As expected, the ribbon samples have siginficantly higher coercivities. The ribbons which were amorphous in the as-spun state had significantly lower Curie temperatures after crystallization than the as-cast samples. This is believed to be due to a difference in the site occupation preferance in ribbons which were amorphous and subsequently crystallized and those which were microcrystalline as-spun. A $Sm_8Fe_{84}Ti_8$ ribbon sample which was microcrystalline as-spun had a T_c approximately equal to the T_c found in the corresponding bulk samples. Mössbauer studies are needed to confirm the preferred site occupations of the constituent atoms of the unit cell in each sample.

The problem seen thus far in these materials is that samples sufficiently free of impurity phases which decrease the hard magnetic properties have not successfully been made. The presence of α-Fe which is a magnetically soft bcc phase allows the domain walls to move easily in these alloys, which leads to the low coercivities found (low in comparison to the 2:14:1 ribbons). A possible way to remove impurity phases from these alloys would be to vary the composition until a pure 1:12 phase is found. Some work has been completed in this area with limited success. By varying the compostion of Sm-Fe-Ti samples, coercivities of 2kOe have been obtained, but α-Fe is still found to precipitate upon heating the sample. Since the presence of α-Fe seems to be dependent upon the processing of the samples, a proper heat treatment should be found which prevents the soft phase from forming. Hovever, this may prove to be extremely difficult since α-Fe is found to begin forming at temperatures lower than the crystallization temperature of the ribbons.

Samples that were heat treated for greater than five minutes had low coercivities, large grain sizes (1000-2000Å), and had relatively high amounts of α-Fe present in comparison to samples with short heat treatment times. The amount of α-Fe present also was found to increase with higher heat treatment temperatures. One possible method for heat treatment would be to "flash anneal" the ribbons. This method involves heating the ribbon sample above the crystallization for a short time (a few seconds) and then rapidly cooling to room temperature, thus the name "flash annealing". This possibility will be investigated in the future.

Another method which may prove to be successful in obtaining high coercivities in these alloys is to form a two phase system with a fine distribution of the 1:12 and 2:14:1 phases. This approach known as precipitation hardening has shown some limited success with coercivities in comparison to the $Sm_8Fe_{84}Ti_8$ sample and could lead to high coercivities in future studies because domain wall pinning may be caused by the second phase (2:14:1). This could be done if samples containing low amounts of impurity phases along with the 1:12 and the 2:14:1 phases can be produced.

References

1. B.D. Cullity, "Introduction to Magnetic Materials", Addison-Wesley Publishing Co., (1972).

2. Charles Kittel, Reviews of Modern Physics.**21**(4), 541(1949).

3. G.C. Hadjipanayis, R.C. Hazelton, and K.R. Lawless, Appl. Phys. Lett. **43**, 797 (1983).

4. J.J. Croat, J.F. Herbst, R.W. Lee, and F.E. Pinkerton, J. Appl. Phys. **55**(6), 2078(1984).

5. N.C. Koon and B.N. Das, J. Appl. Phys. **55**(6), 2063(1984).

6. Sumitomo Special Metals Co. Ltd., Osaka, Japan.

7. E.C. Stoner and E.P. Wohlfarth, Phil. Trans. R. Soc. London Ser. A **240**, 599(1948).

8. Brown Jr., W.F., 1957, Phys. Rev. 105, 1479.

9. M. Sagawa, S Fujimura, M. Togawa, H Yamamoto and Y. Matsura, J. Appl. Phys. **55**, 2083 (1984).

10. T.T.M. Palstra, J.A. Mydosh, G.J. Nieuwenhuys, A.M. van der Kroan and K.H.J. Buschow, J. Magn. Mater. **36**, 290 (1983).

11. T.T.M. Palstra, J.A. Mydosh, G.J. Nieuwenhuys, and K.H.J. Buschow, Phys. Ref. **31**, 4622 (1985).

12. J. Desportes, D. Givord, R. Lemaire, and J. Nagai, Physica B, **86-88** (1977) 69.

13. J. Allemand, C. Bertrand, J LeRoy, J.M. Moreau, D. Paccard, L Paccard, M.A. Fremy, and D. Givord "A Search for New Permanent Magnet Materials: Crystallographic and Magnetic Properties of New Compounds", (to be published).

14. W. Xian-Zhong, B. Chevalier, T. Berlureau J. Etourneau, J.M.D. Coey and J.M. Cadogan, J.Less-Common Metals, **138**, 235-240(1988).

15. B. DeMooij and K.H.J. Buschow, Phillips J. Res. **42**, 246-251(1987).

16. F.R. DeBoer, Huang Ying-Kai, D.B. DeMooij and K.H.J. Buschow, Journal of Less-Common Metals, **135**, 199-204(1987).

17. D.B.DeMooij & K.H.J.Buschow, J.Less-Common Metals, **136**, 207-215(1988).

18. K.H.J. Buschow, J. Appl. Phys. **63**, 3130-3135(1988).

19. K. Ohashi, T. Yokoyama, R. Osugi, and Y. Tawara, IEEE Trans. Magn. (to be published).

20. R.B. Helmholdt, J.J.M. Vleggaar, and K.H.J. Buschow, J. Less-Common Metals, **138**, L11-L14(1988).

21. K.H.J. Buschow, and D.B. de Mooij, "Novel Ternary Fe-Rich Rare earth Intermetallics", (to be published).

22. G. C. Hadjipanayis, S.H. Aly, and Shu-Fan Cheng, Appl. Phys. Lett. **51**(24), 2048-2050(1988).

23. Z.R. Zhao, Y.G. Ren, K.D. Aylesworth, D.J. Sellmyer, E.W. Singleton, J. Strzeszewski, and G.C. Hadjipanayis, J. Appl. Phys. **63**(8), 3699-3701(1988).

24. E.W. Singleton, J. Strzeszewski, G.C. Hadjipanayis, and D.J. Sellmyer, "Magnetic and Structural Properties of Melt- Spun Rare-Earth Transition Metal Intermetallics with $ThMn_{12}$ Structure", (to be published)

25. Thomas, & Goringe, "Transmission Electron Microscopy of Materials", John Wieley & Sons, Inc., (1979).

MAGNETIC AND MICROSTRUCTURE PROPERTIES OF RAPIDLY QUENCHED TRANSITION-METAL-RARE-EARTH-INTERMETALLICS WITH $ThMn_{12}$ STRUCTURE

by

ERIC WALTER SINGLETON

B.A., Hastings College, 1986

AN ABSTRACT OF A THESIS

submitted in partial fulfillment of the

requirements for the degree

MASTER OF SCIENCE

Department of Physics

KANSAS STATE UNIVERSITY

Manhattan, Kansas

1988

ABSTRACT

The purpose of this work has been to study the magnetic and stru
properties of melt-spun and as-cast rare-earth transition metal intermetallic
the $ThMn_{12}$ type structure. The samples investigated are $R_8Fe_{84}Ti_8$ with
Y, Sm, Nd, Gd, Dy and $R_8Fe_{76}[V(Mo)]_{16}$ with $R = Y, Sm, Nd$ and Gd. The
ples have been studied with transmission electron microscopy, x-ray diffr
and magnetic measurements. The tetragonal $ThMn_{12}$ type structure was
in all alloys after annealing. Crystallized $Nd_8(Fe_{1-x}Co_x)_{84}Ti_8$ samples ha
been found with the 1:12 structure with a maximum Curie temperature of
for $x = 0.5$. Magnetic phase transitions will be reported from $4.2°K$ to
Coercivities where found to be strongly dependent on the microstructure wi
largest value (2 kOe) found in $Sm-Fe-Ti$ ribbons. The upper value of H_c
because of the presence of α-Fe in crystallized ribbons. The magnetic pro
will be correlated with the microsturcture.